Draft version November 17, 2017
Typeset using LaTeX **twocolumn** style in AASTeX61

PFS SSP: COSMOLOGY PROGRAM

A. Boyle,[1] S. de la Torre,[2] R. de Putter,[3] O. Doré,[3,4] C. Hikage,[5] Y.-P. Jing,[6,7] I. Kayo,[8] E. Komatsu,[1,5] R. Makiya,[1,5] T. Okumura,[9] A. Pisani,[10] A. G. Sánchez,[11] S. Saito,[1] F. Schmidt,[1] M. A. Strauss,[10] T. Sunayama,[5] M. Takada,[5] P. Zhang,[12,7] and G.-B. Zhao[13,14]

[1] *Max-Planck-Institut für Astrophysik, Karl-Schwarzschild-Str. 1, 85741 Garching, Germany*
[2] *Aix Marseille Univ, CNRS, LAM, Laboratoire d'Astrophysique de Marseille, Marseille, France*
[3] *California Institute of Technology, Pasadena, CA 91125, USA*
[4] *Jet Propulsion Laboratory, California Institute of Technology, Pasadena, CA 91109, USA*
[5] *Kavli Institute for the Physics and Mathematics of the Universe, Todai Institutes for Advanced Study, the University of Tokyo, (Kavli IPMU, WPI), Kashiwa, 277-8583, Japan*
[6] *Center for Astronomy and Astrophysics, School of Physics and Astronomy, Shanghai Jiao Tong University, 955 Jianchuan Road, Shanghai 200240, China*
[7] *IFSA Collaborative Innovation Center, Shanghai Jiao Tong University, Shanghai 200240, China*
[8] *Department of Liberal Arts, Tokyo University of Technology, Ota-ku, Tokyo 144-8650, Japan*
[9] *Institute of Astronomy and Astrophysics, Academia Sinica, P. O. Box 23-141, Taipei 10617, Taiwan*
[10] *Department of Astrophysical Sciences, Princeton University, Peyton Hall, Ivy Lane, Princeton, NJ 08544, USA*
[11] *Max-Planck-Institut für extraterrestrische Physik, Postfach 1312, Giessenbachstr., 85741 Garching, Germany*
[12] *Department of astronomy, Shanghai Jiao Tong University, 955 Jianchuan road, Shanghai, 200240, China*
[13] *National Astronomy Observatories, Chinese Academy of Science, Beijing, 100012, China*
[14] *Institute of Cosmology & Gravitation, University of Portsmouth, Dennis Sciama Building, Portsmouth, PO1 3FX, UK*

(Dated: November 17, 2017)

ABSTRACT

With about 100 nights of the cosmology program of the PFS SSP, we aim at achieving two major goals: (1) To rule out the inverted hierarchy of neutrino masses by measuring $\sum m_\nu < 0.1$ eV at the 95% CL, or to determine the total mass of neutrinos if $\sum m_\nu > 0.1$ eV; and (2) To rule out the standard Λ Cold Dark Matter (ΛCDM) paradigm by finding a time evolution of dark energy density (thus ruling out the cosmological constant Λ) or finding evidence for a correction to General Relativity (GR) on cosmological scales, or to confirm ΛCDM with unprecedented precision. We shall achieve these goals by mapping out cosmological distance, the expansion rate of the Universe, and the growth rate of matter density fluctuations as a function of redshift, with only a few percent uncertainty in each of seven redshift bins between $z = 0.6$ and 2.4. We also make the full use of synergy with the imaging data from the HSC SSP; adding the cross-correlation between 3-dimensional galaxy positions from the PFS and weak gravitational lensing shears from the HSC not only improves the constraints on the neutrino mass, dark energy, and modified gravity, but also provides an important cross check of the results if we measure the neutrino mass, or discover time-evolving dark energy or the breakdown of GR on large scales, which would transform our understanding of the Universe.

1. INTRODUCTION

Structure formation in the Universe is a powerful probe of cosmology. With the galaxy redshift survey program of the PFS, we shall address three major questions in modern cosmology and fundamental physics: What is the origin of cosmic acceleration? What is the mass of neutrinos? What powered the Big Bang (what is the physics of inflation)?

Thanks to the large collecting area of the Subaru telescope, the PFS will map the large-scale distribution of galaxies out to a redshift of 2.4 with unprecedented fidelity, i.e., with a high number density over an enormous solid angle and thus volume. The PFS shall enable us to study, for the first time in detail, the *time evolution* of cosmic structures over a wide range of redshifts ($z = 0.6 - 2.4$). This evolution information is crucial for distinguishing between various effects; for example, both the cosmic acceleration and massive neutrinos slow down the structure formation of the Universe, but their time dependence is different. The cosmic acceleration could be explained by a new form of energy called "dark energy", or by a modification of General Relativity (GR) on large, cosmological scales. These can be distinguished by comparing the expansion history and the growth history of cosmic structures as a function of redshift; thus, our strategy for having a wide redshift coverage is ideally suited for addressing these fundamental questions in cosmology and particle physics.

Specifically, the key quantities that will be extracted from the PFS SSP include:

- The angular diameter distances $D_A(z)$ and the Hubble expansion rates $H(z)$ over $z = 0.6 - 2.4$ from the Baryon Acoustic Oscillation (BAO) and th Alcock-Paczyński (AP) effect
- The linear growth rates of matter density fluctuations $f\sigma_8(z)$ over $z = 0.6 - 2.4$ from the Redshift Space Distortion (RSD)
- The overall (broad-band) shape of the galaxy power spectrum over $z = 0.6 - 2.4$
- Higher-order statistics (such as three-point function) to probe the so-called non-Gaussianity, i.e., departures from Gaussian statistics

In addition to having a wide redshift coverage and large solid angle, the PFS SSP benefits tremendously from having weak lensing measurements provided by the HSC SSP. By cross-correlating 3-d galaxy positions from the PFS and weak lensing measurements from the HSC we can determine the connection of galaxies to the underlying dark matter density fields, and this can be used to understand the physics of galaxy formation (so-called "galaxy bias") and reduce the uncertainties in the cosmological inference associated with it. Having both high-quality galaxy redshifts and weak lensing data in the same sky is another unique advantage of the PFS SSP. This synergy is powerful especially when testing GR: 3d galaxy positions tell us how galaxies move in response to gravitational potentials, while lensing tells us how light is bent by gravity. GR makes a specific prediction for how these two gravitational effects are related to each other, which allows us to test GR on scales much larger than the Solar System.

2. LEGACY VALUE OF THE PFS COSMOLOGY PROGRAM

The wide-area PFS cosmology survey enables a broad range of science topics beyond cosmology. In each visit of the PFS cosmology survey fields, we plan to allocate a small fraction of fibers (less than a few % of 2394 fibers) to rare bright objects such as high-z quasars (QSOs) selected from the HSC-Wide survey (Matsuoka et al. 2016), as well as metal-poor K giants selected from the SDSS (Xue et al. 2014). The spectroscopic survey of bright QSOs will explore formation of super massive black holes in connection with galaxy evolution. The measurements of distant K giants will allow us to study the halo structure of our Milky Way out to a few 100 kpc.

The PFS cosmology survey may lead to a serendipitous discovery; we may find star-forming luminous compact galaxies, "green pea" star-forming galaxies, at redshifts higher than found by the SDSS survey (Cardamone et al. 2009). It would be difficult to construct homogeneous spectroscopic samples for such rare objects efficiently by other means.

The PFS cosmology survey footprints have a full overlap with the SDSS survey regions. Although the PFS cosmology survey will primarily measure [O II] emission lines of target galaxies in a narrow range of wavelengths, the spectra at other wavelengths contain useful information. For example, by stacking spectra of PFS-cosmology galaxies in the range of wavelengths corresponding to redshifts of bright SDSS QSOs as a function of the transverse separation from each QSO, we can study Lyman-alpha scattering emission by the intergalactic medium (IGM) (Croft et al. 2016). The PFS redshift survey, when combined with the HSC galaxies, also enables us to study the association of QSO absorber systems (e.g., damped Lyman-α systems, MgII, CIV) with galaxies at high redshifts (Zhu & Ménard 2013).

3. SURVEY STRATEGY

The survey strategy of the cosmology program is simple: we measure redshifts of galaxies such that we have

a fair sample of the underlying distribution of galaxies in a past light-cone volume. The baseline plan is to visit each field-of-view (1 deg^2) within the survey regions twice, with each visit observing for 15 min (900 sec).

To zeroth order, we would select galaxies randomly within each field-of-view. In reality we must take into account at least two factors:

- We must select galaxies in the redshift range of interest, and
- We cannot select galaxies truly randomly as fibers cannot get too close to each other.

The first issue is the "target selection" and will be described in Sec. 3.1. The second issue is the "fiber assignment scheme", and will be described in Sec. 3.2.

3.1. *Target Selection*

The cosmology program demands that we have a well-sampled galaxy distribution with sufficient number densities (high fidelity) over a wide redshift range (long lever arm). We achieve these requirements by targeting [O II] emission-line galaxies (ELG; [O II]$= 3727\AA$) over the optical and near-infrared wavelength coverage of the PFS, i.e., $z = 0.6 - 2.4$. This type of "fast survey" with a large étendue ($A\Omega$) is possible because Subaru is a 8.2-m telescope, and because the PFS has such a large field-of-view. This survey would not be practical with a 4m-class telescope.

We shall select our targets using magnitude and color information from the HSC photometry catalogs (primarily g, r data with the depth of $i \simeq 26$ mag AB at 5σ). The catalogs will be constructed from deep imaging data in the 1400 deg^2 HSC-Wide survey that will have been completed before the PFS survey. The resulting comoving volume of the PFS redshift survey will then be 9.3 (Gpc/h)^3, i.e., more than twice that of the SDSS BOSS survey (Table 1).

We select targets with a blue rest-frame UV slope and prominent [O II] emission whose redshift is such that the Balmer/$4000\AA$ break is beyond the r band, whereas the Lyman break has not yet entered the g band. Thanks to the deep HSC data ($g < 26$), photometric errors in each filter would have a negligible impact on the target selection. For a shallower survey, photometric scatter in the color selection would cause a contamination of fainter galaxies in the target selection. In Takada et al. (2014), we defined a preliminary target selection cut as

$$22.8 \leq g \leq 24.2 \text{ AND } -0.1 < g - r < 0.3 \\ \text{AND NOT } (g > 23.6 \text{ AND } r - i > 0.3)\,, \qquad (1)$$

which was based upon the original COSMOS Mock Catalog (CMC) (Jouvel et al. 2011). The CMC uses [O II] line strengths estimated from physical galaxy parameters such as star formation rates, stellar masses and metallicities determined by 30 passband photometric data in Capak et al. (2007). This selection yields the expected numbers of galaxies detectable at $\geq 8.5\sigma$ given in Table 1 and shown in the right panel of Fig. 1 as the dashed black line.

The estimate of PFS's instrument throughput has become slightly degraded since Takada et al. (2014). As a result, the same target criteria with the original CMC yield a smaller number density (see the black dotted line in the right panel of Fig. 1). The impact of the new throughput is particularly significant at $z \approx 1.5$. This redshift corresponds to the border between the red and near-infrared arms (Fig. 2). Fortunately this is a fairly narrow feature and thus the effect can be reduced by avoiding this narrow redshift region.

We have been working on improving the COSMOS catalog (Saito et al., in prep) and hence our selection since Takada et al. (2014). The update uses new photometric data (COSMOS2015 in Laigle et al. (2016)), which eliminates contamination in the i band-selected galaxy sample of Capak et al. (2007), and is carefully calibrated against the [O II] flux measurements in zCOSMOS ($0.5 \lesssim z \lesssim 1.5$) and 3D-HST ($2.0 \lesssim z \lesssim 3.5$). In addition, the updated catalog has been validated by the latest [O II] luminosity functions determined over a wide redshift range, $0 \lesssim z \lesssim 2.5$.

When applying the Eq. 1 cuts to the new CMC, we obtain the cyan line in the right panel of Fig. 1, which results in a significant reduction in the expected numbers of galaxies particularly at high redshifts, $z \geq 1.3$. This is due to a combination of two factors: the difference in the instrument throughput estimates between now and Takada et al. (2014), and the difference between the two CMC catalogs. In fact, the former contribution dominates: the difference between the cyan and black dotted lines in the right panel of Fig. 1 is much smaller than that between the black dashed and dotted lines.

An adjustment of the magnitude and color cuts based on the new CMC is small. The new cuts are

$$23.2 \leq g \leq 24.1 \text{ AND } 0 < g - r < 0.35, \qquad (2)$$

which are shown by the red rectangle in the left panel. The expected number densities using the new CMC and new cuts are shown by the red solid line in the right panel of Fig. 1, which is fairly close to the cyan line.

Given the low success rate in these selection cuts ($\lesssim 50\%$), one possibility is to lower the conservative 8.5σ threshold of signal-to-noise. Here we demonstrate the case with a 6σ threshold. The blue lines in Fig. 1 show

PFS Cosmology Survey Parameters (Takada et al. 2014)

redshift	$V_{\rm survey}$ $[{\rm Gpc}/h]^3$	N_g per field	$\bar{n}_g$ $[10^{-4}(h/{\rm Mpc})^3]$	bias b_g	$\bar{n}_g P_g(k)$ $k=0.1h/{\rm Mpc}$	$\bar{n}_g P_g(k)$ $k=0.2h/{\rm Mpc}$
$0.6<z<0.8$	0.59	85	1.9	1.18	0.74	0.25
$0.8<z<1.0$	0.79	358	6.0	1.26	2.23	0.74
$1.0<z<1.2$	0.96	420	5.8	1.34	2.10	0.68
$1.2<z<1.4$	1.09	640	7.8	1.42	2.64	0.87
$1.4<z<1.6$	1.19	491	5.5	1.50	1.78	0.59
$1.6<z<2.0$	2.58	598	3.1	1.62	0.95	0.31
$2.0<z<2.4$	2.71	539	2.7	1.78	0.76	0.25

Table 1. From the left: redshift range of each slice, comoving volume (V), the number of [O II] galaxies per field (N_g), the mean comoving number density ($\bar{n}_g$), the linear bias parameter (b_g) and the values of $\bar{n}_g P_g(k)$ at $k=0.1$ and $0.2h$/Mpc. A survey area of 1464 deg^2 is assumed. For comparison, the BOSS BAO survey samples 10000 deg^2 over $0.4<z<0.7$, $V_{\rm survey}=4.4$ $({\rm Gpc}/h)^3$, $\bar{n}_g = 3\times10^{-4}(h/{\rm Mpc})^3$, $b_g=2.3$ and $\bar{n}_g P_g(k=0.1\ h/{\rm Mpc})\simeq 5$.

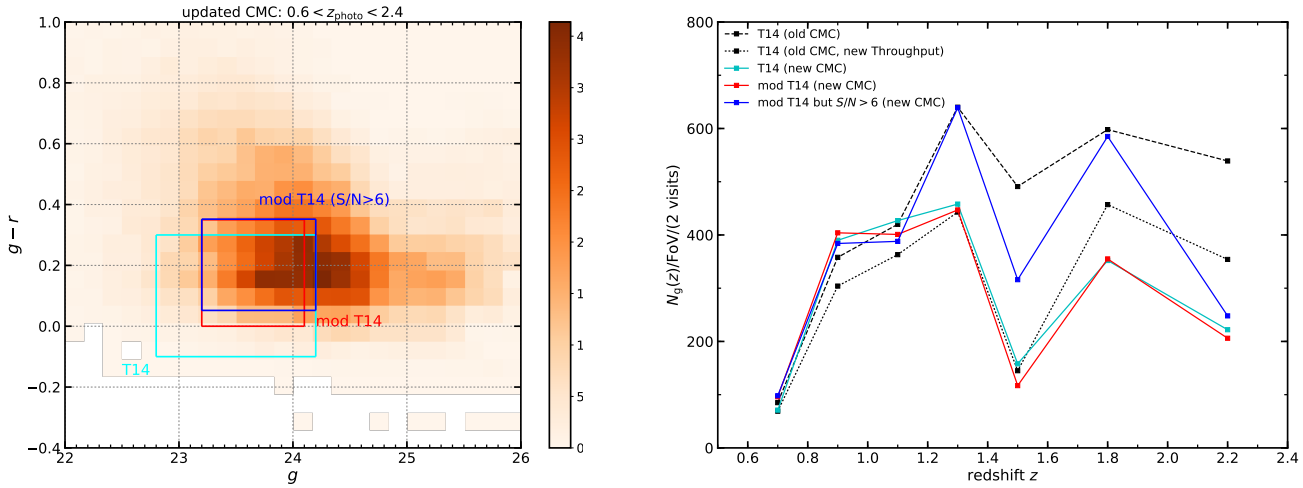

Figure 1. (Left) Distribution of detectable [O II] emitters in the improved COSMOS Mock Catalog (Saito et al. in prep.) on the color-magnitude diagram. We show the number of objects in each cell that are $0.6<z<2.4$ ELGs with [O II] emission detectable at $\geq 6\sigma$ in a 15 min exposure. The cyan rectangle shows the selection cut used by Takada et al. (2014), which was based on the original COSMOS Mock Catalog (Eq. 1). Our ongoing studies on cuts informed by the updated COSMOS Mock Catalog are also shown; the red rectangle shows Eq. 2 which is closer to the peak of the distribution of the updated catalog, while the blue rectangle covers a wider area in the (g, $g-r$) space but adopts the lower signal-to-noise threshold of 6σ than 8.5σ in Takada et al. (2014). (Right) The expected number of galaxies in each field-of-view (after two visits) per redshift bin. The black dashed line shows those in Table 1, while the other lines with various colors show new estimates using the cuts shown in the left panel with the same colors respectively. The black dotted line shows the expected number density when we adopt the original CMC but with the new instrument throughput, showing the impact of the instrumental degradation on the target selection. The dip at $z\approx 1.5$ is due to the border between the red and IR arms (Fig. 2).

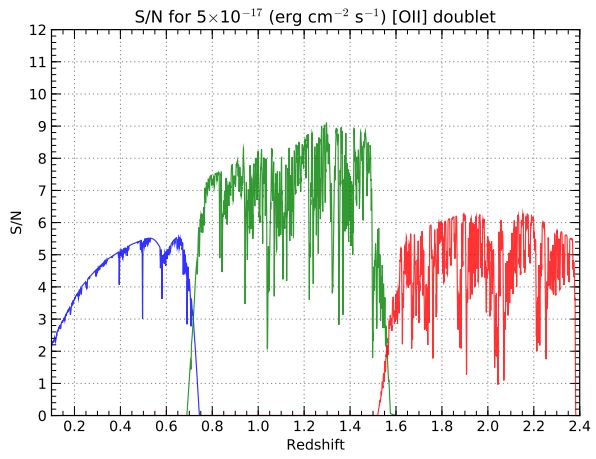

Figure 2. Expected signal-to-noise ratio (S/N) for measuring the [O II] emission line as a function of redshift. The blue, green and red curves show the results for the PFS blue, red and IR arms, respectively, for a total emission line flux of 5×10^{-17} erg/cm^2/s. This computation assumes 15 min total exposure (split into two exposures; 450sec $\times$ 2), $\sigma_v = 70$ km/s for the velocity dispersion (the intrinsic line width), and $0.8''$ for the seeing FWHM. We also accounted for the finite galaxy size relative to the seeing profile and the fiber size, assuming an exponential profile with scale radius $0.3''$ for the emission-line region (about 3.5 kpc/h for a galaxy at $z = 1$). Note that S/N is estimated by the root-sum-square of the spectral pixels (i.e., it is a matched filter combining both doublet members).

the adjusted magnitude-color cut for the 6σ case:

$$23.2 \leq g \leq 24.2 \text{ AND } 0.05 < g - r < 0.35, \quad (3)$$

and the resultant number density of galaxies. In this case, the success rate becomes as high as $\sim 62\%$ and the selection recovers the number density in Takada et al. (2014) at some redshift bins.

We admit that these studies are still uncertain, and there is no doubt that our selection cuts will be revised once the PFS survey begins in 2020. First, it is likely that the commissioning data can be used to redefine our target selection cuts. Second, we plan to use the first few nights of the Cosmology program for pilot surveys to refine the cuts. In addition, the Galaxy Evolution program will yield much improved physical parameters of the [O II] galaxies, and such information can be used to further refine the cuts, and improve modeling [O II] emission in galaxies in collaboration with the Galaxy Evolution team.

We continue to use the original survey parameters given in Takada et al. (2014) throughout the rest of this report.

3.2. *End-to-end Simulation*

We have run many realisations of "end-to-end simulations" going from simulated 3-dimensional positions of galaxies in redshift space to the cosmological parameters, to assess the realistic capability of the PFS cosmological program to constrain the key cosmological quantities of interest such as the total mass of neutrinos and the dark energy parameters.

Specifically, we used log-normal simulations in redshift space that were developed at MPA[1] (Chiang et al. 2013; Agrawal et al. 2017) to generate positions and velocities of galaxies. We then calculate the monopole and quadrupole power spectra from these mock galaxy catalogs, and estimate the cosmological parameters using the Markov Chain Monte Carlo (MCMC). Fig. 3 shows the monopole and quadrupole power spectra measured from one realisation of the simulation in a redshift slice of $1.4 < z < 1.6$, combining spectra from both survey regions. These data represent accurately the quality of data we expect from the survey.

So far we assumed that we would select galaxies randomly to have a fair sample of the underlying distribution of galaxies. In practice, however, this is not quite possible because fibers cannot get too close to each other. We must assign fibers such that fibers do not collide. Since we have only two visits per field-of-view, the fiber collision constraint implies that we do not have quite a fair sample of galaxies in the over-dense region. This would then result in an underestimate of the underlying clustering strength of galaxies.

The PFS collaboration uses a software called "Exposure Targeting Software (ETS)" developed at MPA[2] to decide how to assign fibers to targets within a given field-of-view. There are three options for the fiber assignment: "naive", "draining", and "new". The "naive" method simply assigns a fiber to its nearest target, and is often called the "greedy algorithm" in computer science. The "draining" method (Morales et al. 2012) also assigns a fiber to its nearest target, but a fiber with the fewest targets within its reach is given priority to observe a given target[3]. The "new" method is an experimental method that attempts to observe more targets in denser regions. Given the simplicity of the survey strategy of the cosmology program, all methods yield

[1] Available as "lognormal_galaxies" at http://wwwmpa.mpa-garching.mpg.de/~komatsu/codes.html

[2] Available at https://github.com/Subaru-PFS/ets_fiber_assigner

[3] This is the-poorest-gets-it-first approach. It first creates a list of targets within the patrol area of a given fiber, and repeats this for all fibers. It then assigns a target to a fiber which has the *shortest* list.

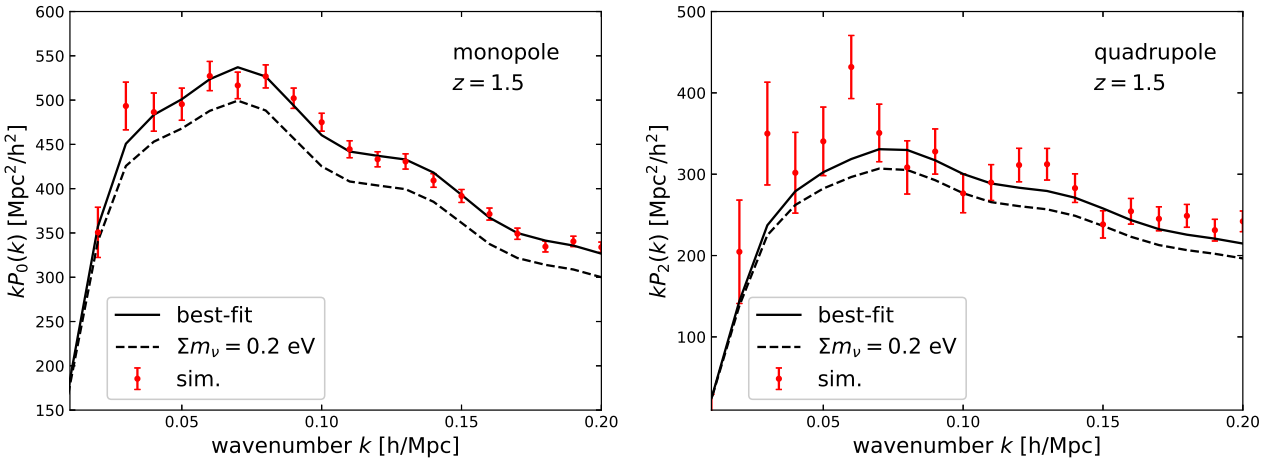

Figure 3. (Left) Monopole power spectrum at $1.4 < z < 1.6$ from one realisation, combining the data in both fields of the cosmology program. The solid line shows the best-fitting power spectrum, while the dashed line shows the power spectrum for $\sum m_\nu = 0.2$ eV. The input neutrino mass for the simulation is $\sum m_\nu = 0.06$ eV. The error bars are calculated from 1000 realisations. (Right) Same as the left panel but for the quadrupole power spectrum.

similar results; thus, we report on the results with the "naive" method.

The left panel of Fig. 4 shows the distribution of galaxies selected by the ETS after two visits per field-of-view, together with hexagons showing fields-of-views. The right panel shows the ratio of the two-point correlation function of galaxies selected by the ETS to the underlying one. For this study we used an N-body simulation run with the "HACC" code (Sunayama et al. 2016). The redshift of the snapshot is $z = 0.8$ and the depth is 2 Gpc/h, while the sky area used for this analysis is about 150 deg^2. We find that the fiber assignment produces a small, but visible, effect on the correlation function, reducing its amplitude uniformly by less than 0.2% at $r > 10$ Mpc/h and by somewhat larger amount at smaller separations. The impact of the fiber assignment is thus limited, and is correctable.

4. SCIENCE GOALS

4.1. *Neutrino Mass*

Massive neutrinos slow down growth of the cosmic structure (Lesgourgues & Pastor 2006). Their large velocity dispersion, $\sigma \approx 1800(1+z)(0.1\text{ eV}/m_\nu)$ km/s, makes their contribution to the gravitational potential via the Poisson equation small, with only a part of the total matter (baryons Ω_b and cold dark matter Ω_c) contributing to the Poisson equation. Growth of the density fluctuations is suppressed in proportion to Ω_ν/Ω_M (with $\Omega_M = \Omega_c + \Omega_b + \Omega_\nu$) below the so-called neutrino free streaming length, which is approximately the velocity dispersion times the Hubble time, $a/k = \sqrt{2/3}\sigma/H \approx 39(0.1\text{ eV}/m_\nu)[\Omega_M h^2(1+z)/0.14]^{-1/2}$ Mpc. Here, a is the scale factor and k is the comoving wavenumber, and thus a/k is a physical length of free-streaming. This leads to a *scale- and time-dependent suppression* of the matter power spectrum relative to that with massless neutrinos. Having a long lever arm in both spatial scales and redshifts is thus important for improving upon the neutrino mass constraint, and the PFS galaxy survey does precisely that.

Fig. 3 shows how the massive neutrino suppresses the monopole (left) and quadrupole (right) power spectra. The density parameter of massive neutrinos, Ω_ν, is proportional to the sum of all neutrino masses and is given by $\Omega_\nu h^2 = \sum m_\nu/93$ eV; thus, the galaxy power spectrum primarily constrains $\sum m_\nu$ rather than individual masses. (In principle the shape of the power spectrum is sensitive to individual masses, the effect is likely too small to be useful for the mass ranges that are favored today.) In addition the neutrino mass changes the expansion rates (hence the angular diameter distances) in a late time universe, which also affect the monopole and quadrupole power spectra.

We use all the information; namely, the BAO and the AP effect probing the expansion history, the RSD probing the growth of structure, and the shape of the galaxy power spectrum probing the suppression of the power due to neutrino free-streaming. Fig. 5 shows how each element constrains the neutrino mass. This calculation is based on a simple Fisher-matrix approach (Boyle and Komatsu, to be submitted). We find that the RSD dominates the constraint. We also find that the constraint

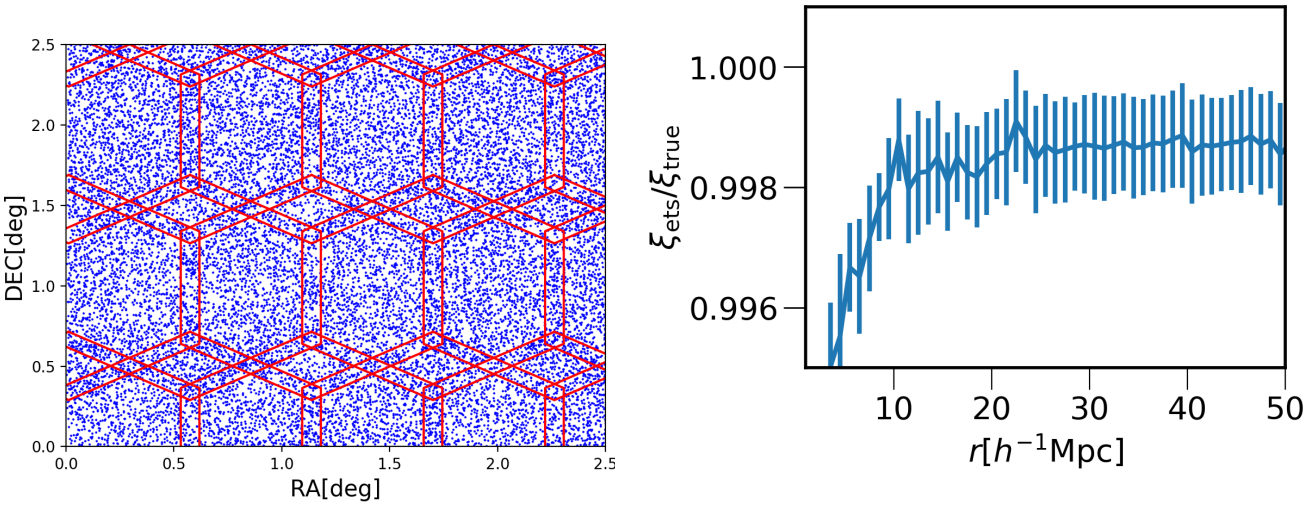

Figure 4. (Left) Distribution of galaxies selected by the ETS after two visits. The hexagons show the tiling pattern. The redshift of the simulation is $z = 0.8$ and the depth is 2 Gpc/h. (Right) Ratio of the correlation functions of galaxies in real space selected by the ETS after two visits shown in the left panel to that of the original catalog before selection. The error bars in different radial bins are correlated. The cosmic variance cancels largely in the ratio.

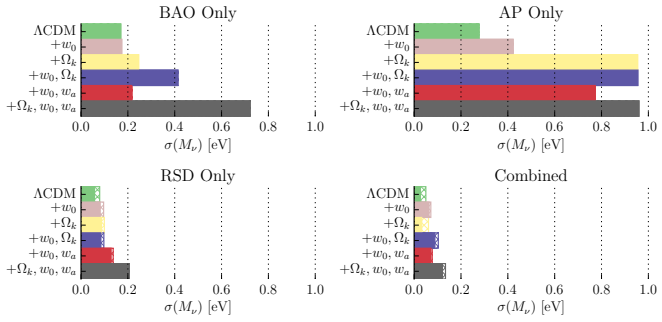

Figure 5. Fisher-matrix-based calculations of the expected 68% CL neutrino mass constraints from the PFS data combined with the Planck CMB data. The top-left and top-right panels show the constraints from the expansion history of the Universe probed by the BAO and the AP effect, respectively, whereas the bottom-left panel shows that from the growth of structure probed by the RSD. The bottom-right panel shows the combined constraints. In the bottom panels, the hatched bars show the constraints with the prior on the optical depth τ from the Planck data, whereas the solid bars show the constraints when τ is known perfectly. The expansion history constraints are not affected by τ.

depends on the assumed cosmological model. While the scale-dependent suppression of the power spectrum gives a robust constraint that is independent of the assumed cosmological model, the constraining power is not as strong as the RSD. Our goal is to achieve $\sum m_\nu < 0.1$ eV (95% CL) *within the context of the standard ΛCDM model*.

Fig. 6 shows the parameter constraints from one realisation of the end-to-end simulation. We use the power spectra up to $k = 0.2$ h/Mpc, and linear bias parameters at each redshift are marginalised over. As the power spectra of log-normal realisations agree statistically with the input spectra, the simple linear bias model without the Fingers-of-God (FoG) effect retrieves the correct cosmological parameters. We find that the expected constraint on the sum of neutrino masses is $\sum m_\nu < 0.1$ eV (95% CL). We shall address the impact of a more complex non-linear power spectrum model in Sec. 4.2.

Achieving the threshold of 0.1 eV is important. While we know that neutrinos have masses, we do not know the absolute value of the masses. The neutrino oscillation experiments show that there are two possibilities for the *mass hierarchy* of neutrinos (Mohapatra et al. 2007):

- The normal hierarchy, in which one neutrino mass eigenstate is heavier than the other two eigenstates, and
- The inverted hierarchy, in which two neutrino mass eigenstates are heavier than the third mass eigenstate.

The minimum total mass of the normal hierarchy is $\sum m_\nu^{\rm normal} \approx 0.06$ eV, while that of the inverted hierarchy is $\sum m_\nu^{\rm inverted} \approx 0.1$ eV; at 2σ, an upper bound of $\sum m_\nu < 0.1$ eV would rule out the inverted mass hierarchy. If the hierarchy is the inverted one, then the PFS would measure, for the first time, the total neutrino mass from the cosmological data sets. *Either way, such findings would have profound implications for cosmology and particle physics*, and the PFS will be in a good position to have a high impact.

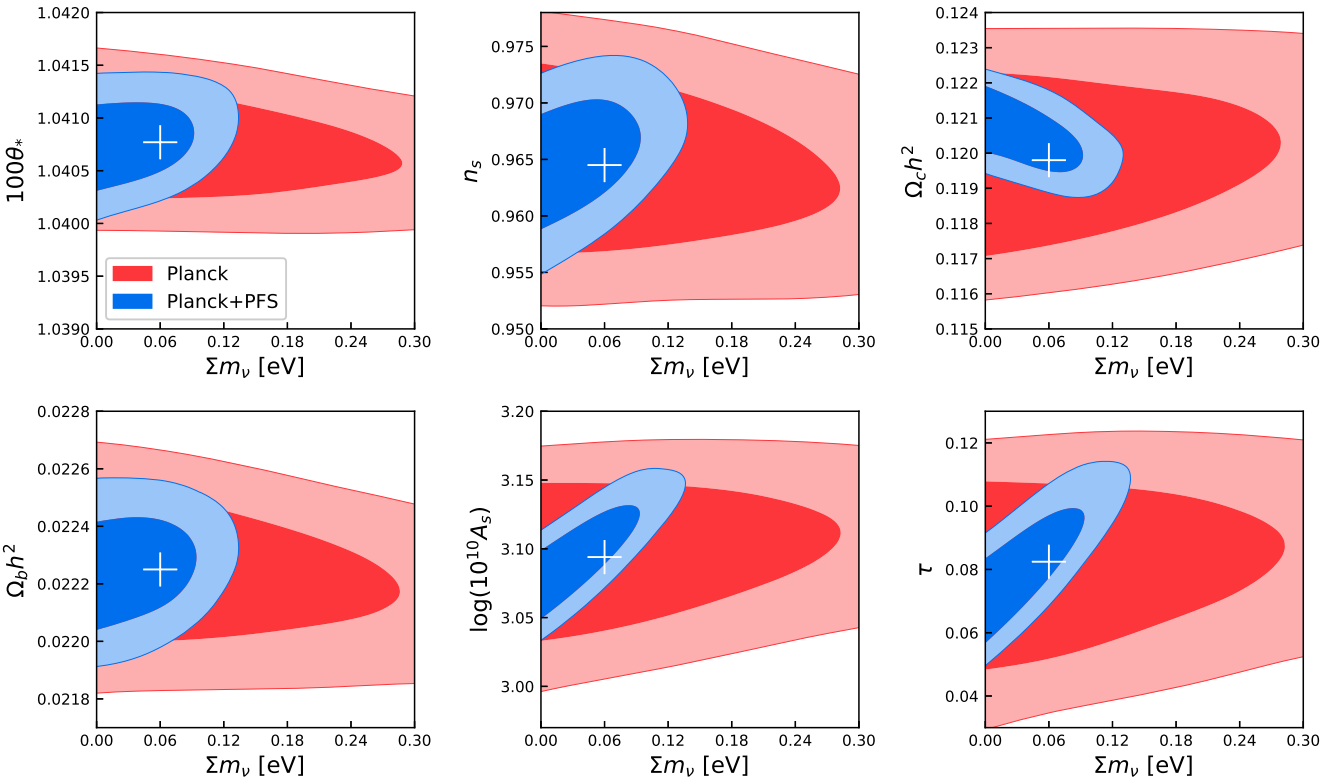

Figure 6. Parameter constraints from one realisation of the end-to-end simulation. The red contours show the 68% and 95% CL constraints from the Planck data, while the blue contours show the expected combined constraints from Planck and PFS. The crosses show the input parameters. Dark energy is assumed to be a cosmological constant.

Deciding the mass hierarchy sets a concrete target for the neutrinoless double-β decay experiment, which will distinguish between Dirac-type and Majorana-type neutrinos. If neutrinos are Majorana, ruling out the inverted mass hierarchy implies $m_{\beta\beta} \lesssim 0.02$ eV (95% CL) for neutrinoless double-β decay experiments. This too carries fundamental importance in particle physics.

The constraint on the neutrino mass can be improved further by adding weak lensing data from the HSC (Sec 5), and by having a better measurement of the optical depth of the CMB by reionisation, τ (Allison et al. 2015). The latter helps because of the following reason. The CMB power spectrum at high multipoles ($\ell > 10$) depends on the primordial scalar amplitude A_s attenuated by $\exp(-2\tau)$, hence the combination $A_s \exp(-2\tau)$. On the other hand, the RSD measures the amplitude of fluctuations in a late time universe, and comparing it with the primordial amplitude A_s gives a constraint on the neutrino mass. We therefore need an estimate of τ to break this degeneracy. While the large angular scale polarisation data of the CMB give an estimate of τ, the current estimates by WMAP and the two instruments on board Planck do not quite agree and there is a debate as to which value is the correct estimate. This uncertainty limits our ability to constrain $\sum m_\nu$. We find that the PFS can constrain a combination $F \equiv \tau/(0.28\sum m_\nu + 0.068)$ (where $\sum m_\nu$ is in units of eV) rather well: $F = 1.00 \pm 0.11$ (68% CL) and $0.80 < F < 1.22$ (95% CL). To first order in the uncertainties, we have

$$\frac{\delta F}{F} = \frac{\delta\tau}{\tau} - \frac{\delta(\sum m_\nu)}{\sum m_\nu + 0.243}\,. \tag{4}$$

This means that the uncertainty in τ would be subdominant if it is determined to be better than 10%. We also demonstrate the sensitivity to τ in the bottom panels of Fig. 5.

In addition, higher-order statistics such as the three-point function (bispectrum) of galaxies can help determine the amplitude of matter fluctuations (hence the neutrino mass), especially at high redshifts where the lensing data have low signal-to-noise ratios. N. Sugiyama is currently calculating the expected improvements in the neutrino mass and dark energy when the galaxy bispectrum is included. Since the galaxy bispectrum is sensitive to non-linear structure formation and galaxy bias (see, e.g., Sefusatti & Komatsu 2007), in-

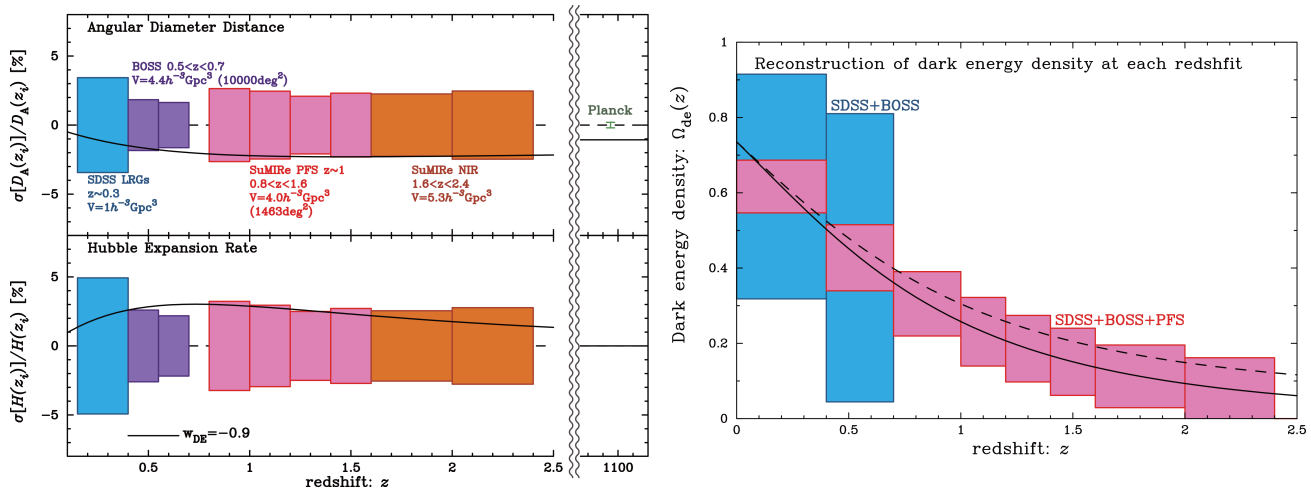

Figure 7. (Left) Fractional 1σ errors of determining the angular diameter distance and the Hubble expansion rate from the PFS survey. The solid curve in each panel shows the effect of $w = -0.9$. (Right) Reconstruction of the fractional dark energy density parameter at each redshift, $\Omega_{\rm de}(z) \equiv \rho_{\rm de}(z)/[3H^2(z)/8\pi G]$, assuming a flat universe. The solid curve shows the energy density parameter for the fiducial ΛCDM model, while the dashed curve shows the redshift evolution for an early dark energy model in Doran & Robbers (2006) with $w_0 = -1$ and $\Omega_d^e = 0.05$.

cluding its measurement could break degeneracies with bias parameters and further improve expected neutrino mass constraints.

4.2. *Impact of Non-linear Power Spectrum Model*

In the previous section we used the simplest model of the galaxy power spectrum (i.e., linear matter power spectrum, linear galaxy bias, and linear RSD) to predict PFS's ability to constrain the neutrino mass. In this section we address the impact of non-linearities, based on Sánchez et al. (2017); namely, we marginalise over non-linear galaxy bias (b_2), non-local bias arising from tidal fields (γ_3^-), and non-linear RSD from the FoG ($a_{\rm vir}$). Doing so degrades the bound on the neutrino mass by a factor of two: $\sum m_\nu < 0.24$ eV (95% CL).

We find that this is largely due to the FoG. Our FoG model is based upon the model to describe Luminous Red Galaxies (LRGs) in the BOSS data (Sánchez et al. 2017). It is known that LRGs reside in massive halos and thus possess rather large FoG effects. On the other hand, emission-line galaxies reside in less massive halos and would show little FoGs: this has been seen by DEEP2 (Coil et al. 2008), GALEX-subsample of the SDSS galaxies (Zehavi et al. 2011), and WiggleZ (Contreras et al. 2013). Not marginalising over the FoG parameter $a_{\rm vir}$ brings the expected upper bound back to 0.1 eV.

4.3. *Dark Energy*

Dark energy changes the angular diameter distance D_A, the expansion rate H, and the growth rate of structure. The left panel of Fig. 7 shows the expected constraints on D_A and H over a wide range of redshifts measured by PFS. These constraints come from the BAO and the AP effect.

It is common to parameterize the property of dark energy using the equation of state parameter w. While low-z surveys perform better in standard forecasted w constraints, this is based on the assumption of a near-constant evolution of w throughout the Universe's history. This assumption needs to be tested using constraints at higher redshifts. PFS is the unique survey to do that. We make this point by a direct reconstruction of the dark energy density parameter Ω_{de} as a function of redshift (right panel). In addition to extending the measurements to $z \simeq 2$, the PFS data improve the precision at low redshifts as $D_A(z)$ at high z arises from an integration of $1/H(z)$. With such measurements of the evolution of dark energy density over a wide redshift range, we can test whether dark energy is a cosmological constant.

Thanks to a wide redshift coverage, PFS can constrain w (from time dependence of Ω_{de}) and $\sum m_\nu$ simultaneously. Fig. 8 shows the expected constraints from one realisation of the end-to-end simulation combined with the Planck data. We use the power spectra up to $k = 0.2$ h/Mpc, and linear bias parameters at each redshift are marginalised over. Adding Type Ia supernova data such as the Joint Light curve Analysis (JLA) does not change the constraint very much, indicating that the statistical power of the PFS as a dark energy probe is high. We find that PFS can achieve an upper bound of $\sum m_\nu < 0.2$ eV (95% CL) when w is allowed to vary.

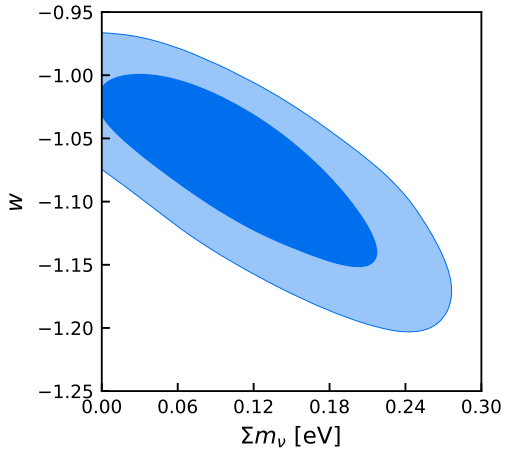

Figure 8. Expected 68% and 95% CL joint constraints on w and $\sum m_\nu$ from one realisation of the PFS data combined with the Planck data.

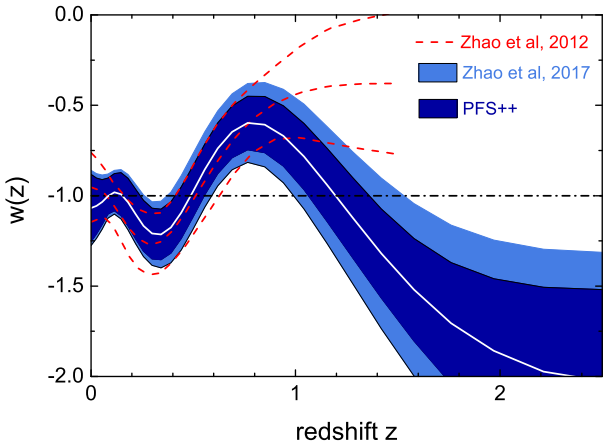

Figure 9. Reconstructed evolution history of the dark energy equation of state using the current observations (Zhao et al. 2017) compared with the 2012 result (Zhao et al. 2012) as well as the forecasted uncertainty for the PFS data. The red lines show the mean and the 68% CL of the 2012 data, the white line and the light blue band show those of the current data, and the light blue band shows the 68% CL region of the PFS data. The last two also include the constraints from the Planck CMB, the JLA supernova, the BOSS DR11 Lyman-alpha BAO, and the BOSS DR12 galaxy BAO data.

The bottom right panel of Fig. 5 also shows how the neutrino mass constraint is affected when we vary the background cosmological model. The PFS would not be able to reach a threshold of 0.1 eV for various extensions of the ΛCDM model.

Still, interesting physics of dark energy may be hidden when we measure the dark energy densities; namely, the equation of state may oscillate around $w = -1$ giving, on average, regular dark energy evolution consistent with a cosmological constant. Indeed there is significant theoretical motivation for dark energy potentials with periodic modulations (Frieman et al. 1995; Dodelson et al. 2000; D'Amico et al. 2016; Schmidt 2017). These can arise through non-perturbative effects, when a continuous shift symmetry of the field driving acceleration is broken to a discrete symmetry. This is analogous to axion monodromy in models of string inflation (Silverstein & Westphal 2008; McAllister et al. 2010).

A concrete realization, "monodromic k-essence", was recently proposed by Schmidt (2017). This model, which employs a non-standard kinetic term (which also frequently occurs in string inflation models), exhibits an equation of state which oscillates around a mean equation of state close to −1, where the amplitude and frequency of oscillations are free parameters.

The most prominent signatures of the oscillations appear in observables which are not integrated, in particular the Hubble rate, which is accessible to PFS through radial BAO and AP measurements. Interestingly, Zhao et al. (2017) have found hints of a time-varying dark energy equation of state with oscillatory features. If this is due to a dark energy with oscillations, PFS could conclusively confirm this (see Fig. 9).

4.4. *Modified Gravity from RSD*

The cosmic acceleration may not be due to dark energy, but to a modification of gravity on large scales. The growth rate of structure can be used to test this. Fig. 10 shows the expected constraints on the linear growth rate of the structure, $f\sigma_8$, as a function of redshift as well as the existing constraints from various galaxy surveys. The PFS will extend the measurements of $f\sigma_8$ into the hitherto uncharted redshift range, providing a powerful test of GR on cosmological scales. The dashed line shows an example prediction from the so-called "nDGP+DE" brane-world model. This model is based on the normal branch of the DGP braneworld model (Dvali et al. 2000), with a quintessence-type dark energy component added on the brane, so that the expansion history coincides with flat ΛCDM (Schmidt 2009). This can be seen as a simplified stand-in for more realistic braneworld or massive-gravity models. This model, with parameter $r_c H_0 = 1$, is still allowed by current BOSS data at 2σ (Barreira et al. 2016). The PFS can rule out (or confirm!) this model decisively.

The effect of modified gravity is often parameterized by the "growth index" γ, which is defined as $f(z) = \Omega_M^\gamma(z)$. As $\Omega_M(z)$ approaches unity at high redshifts, this parameterization is not suitable for the PFS whose strength lies at high redshifts. For this reason the ex-

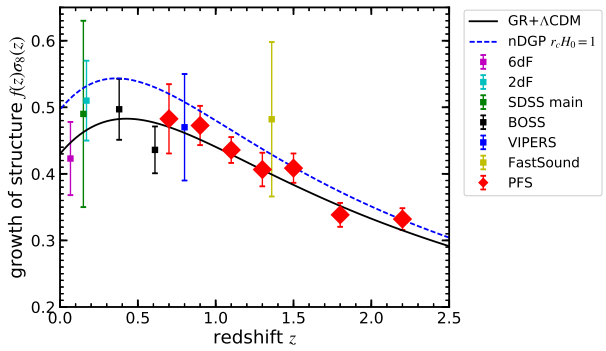

Figure 10. Expected 1σ constraints on $f\sigma_8$ from one realisation of the PFS data combined with the Planck data, as well as the current constraints. The blue line shows the example prediction of a model of modified gravity called "nDGP+DE".

pected constraint on γ from the PFS is not much better than the existing constraint from the BOSS data.

The weak lensing data of the HSC as well as the CMB lensing data of the Atacama Cosmology Telescope (ACT) offer another test of modified gravity models. Lensing and galaxies form a "powerful duo": seeing the effects of modified gravity in *both* galaxy motion traced by the RSD and bending of light traced by lensing greatly enhances our confidence in such a groundbreaking discovery. We shall address synergy with the lensing data in Sec. 5.

4.5. *Non-Gaussianity*

The non-Gaussianity of primordial fluctuations is a powerful probe of the physics of inflation (Bartolo et al. 2004). The most promising observable is the bispectrum of primordial curvature perturbations, i.e., the Fourier transform of the three-point correlation function, which vanishes for Gaussian initial conditions. The bispectrum depends on three wavenumbers k_1, k_2, and k_3, and potentially encodes a rich set of primordial physics (Komatsu et al. 2009). Particularly interesting is the so-called "squeezed configuration", in which one of the wavenumbers is much smaller than the other two, $k_1 \ll k_2 \approx k_3$. Standard inflation models based upon a single energy component (single field) cannot generate a signal in this configuration of the bispectrum. We can test this using the PFS data, using both the two-point (power spectrum) as well as higher-point statistics of PFS galaxies. The amplitude of the squeezed bispectrum is usually parameterised by the parameter $f_{\rm NL}$. A detection of non-zero $f_{\rm NL}$ would rule out the entire paradigm of standard single-field slow-roll inflation.

To this end we use the newly developed "position-dependent power spectrum" (Chiang et al. 2014, 2015). This is one of the most promising tools for galaxy surveys because it is easy to measure and model (the effects of non-linear matter evolution and galaxy biasing are easier to understand in the squeezed configuration). Based on the Fisher matrix calculation, the expected 1σ error bar on $f_{\rm NL}$ from PFS using this technique is $\Delta f_{\rm NL} \approx 5$. This is comparable to the best CMB constraint to date from Planck CMB data (Planck Collaboration et al. 2016), but using a completely independent probe, and using different spatial scales. Given that primordial non-Gaussianity could be scale dependent, the PFS constraints should be seen as complementary to the CMB.

A squeezed primordial bispectrum also changes the galaxy power spectrum on large scales (Dalal et al. 2008). The expected 1σ error bar from the PFS power spectrum is $\Delta f_{\rm NL}^{\rm local} \approx 12$.

Other interesting inflationary physics is encoded in the "equilateral shape", which peaks when $k_1 \approx k_2 \approx k_3$. The effect of this type of primordial non-Gaussianity is more challenging to measure and model. Work on quantifying PFS's ability to constrain the amplitude of this shape is in progress.

4.6. *Cosmic Voids*

Cosmic voids, the under-dense regions of the Universe, are a novel tool to constrain cosmological parameters. In attempting to explain the accelerated expansion of the Universe – which began at a low density state of the Universe – modified gravity models modify GR at large scales and in the low density regime. In this framework voids are an optimal environment to test cosmological models and modified gravity theories, as the effects of such modifications would be maximal.

Among different void applications, the void abundance constrains the dark energy equation of state and gravity models (e.g., Pisani et al. 2015; Cai et al. 2015), while the analysis of void shape – with the AP test on void stacks and RSD around voids – constrains Ω_M and measures the growth rate of structures at a level that is competitive with the state-of-the-art constraints from standard RSD (see, e.g., results with voids from BOSS data: Sutter et al. 2014; Hamaus et al. 2016, 2017).

Thanks to the high tracer sampling density at $z \geqslant 1.1$, the PFS dataset will give access to the void hierarchy with unprecedented detail, unlock a high void number density and provide us with accurate information on the smaller scales.

At higher redshift the AP test becomes more powerful in constraining cosmological parameters. We can thus

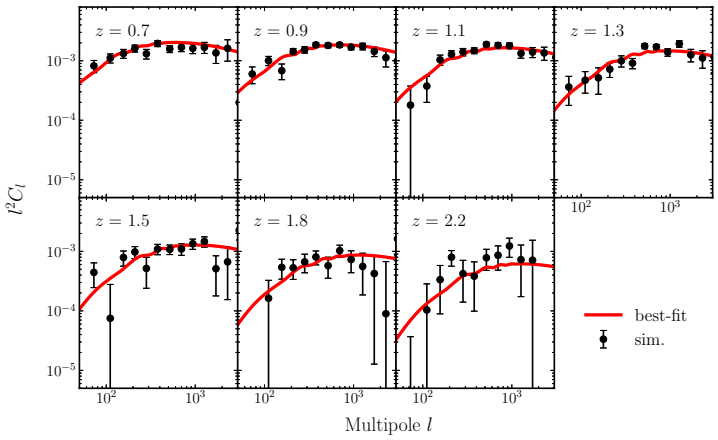

Figure 11. Cross-correlation power spectrum of mock weak lensing data of the HSC and galaxy positions of the PFS from one realisation of the end-to-end simulation. The signal-to-noise ratios up to $\ell = 1000$ are 18.9, 25.6, 22.5, 18.5, 11.73, 8.4, and 6.1 for redshift slices at $z = 0.7$, 0.9, 1.1, 1.3, 1.5, 1.8, and 2.2, respectively.

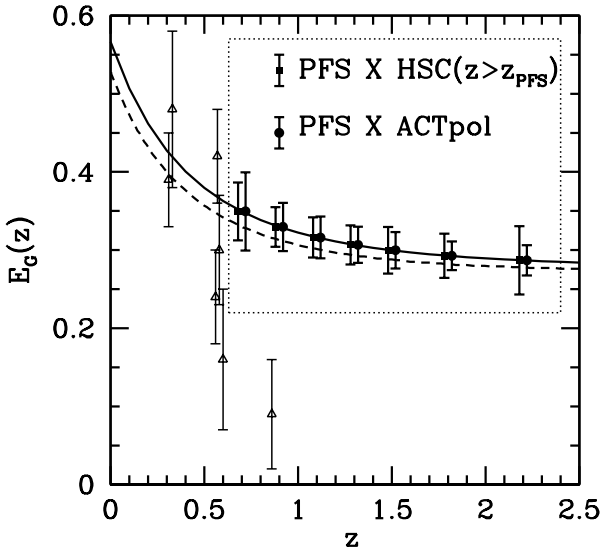

Figure 12. Expected 1-σ error bars of E_G for the PFS in combination with lensing data from HSC and ACT.The dashed line is the prediction of a "nDGP+DE" model described in Sec. 4.4. The E_G measurement can exclude this model at more than 2σ. Existing E_G measurements (open squares) are also included for comparison.

expect a substantial improvement in constraints using PFS voids, all the more since the access to the nested hierarchy of voids and subvoids is a certain asset for the AP measurement. Additionally, with PFS data, a new measurement of the growth rate from RSD around voids can be obtained – for the first time with such high precision at $z \geqslant 1.1$.

Finally, an active field of void science focuses in improving theoretical models of void abundance to be used for cosmological constraints. A high z sample such as the one provided by PFS would be invaluable to improve such models, especially to better model the abundance of smaller voids (that bear a high statistical power).

Because of all the above reasons we can expect the high sampling density of PFS voids to provide stringent limits on deviations from GR and cosmological parameters.

5. SYNERGY WITH HSC AND CMB LENSING

The HSC data not only provide a catalog of galaxies for the PFS, but also weak lensing data that complement cosmological constraints from the galaxy power spectrum of the PFS. In particular, by cross-correlating the HSC weak lensing data with 3-dimensional positions of PFS galaxies, we can measure the galaxy-mass correlation as a function of redshift, i.e., *tomography* of weak lensing data. The PFS and HSC thus form a "powerful duo", which makes the PFS survey unique among the competitors that have either imaging data (lensing) or galaxy positions only.

Fig. 11 shows the cross-power spectrum from one realisation of the simulation. We find that the cross-power spectrum will be detected with high statistical significance. We can also use the auto power spectrum of weak lensing (not shown), and with these together the neutrino mass and dark energy constraints would improve. We have not completed the full parameter forecast yet for PFS+HSC; this is still work in progress, especially in combination with the auto power spectrum.

Nevertheless, the cross-power spectrum offers a powerful test of modified gravity, as discussed below. This point alone fully justifies uniqueness of the synergy between PFS and HSC.

The survey regions of the PFS overlap with those of the on-going and future ground-based CMB experiments, such as the ACT and the Simons Observatory. These data sets provide a mass map of the Universe via weak lensing of the CMB over a broad range of redshifts from $z \approx 0.5$ to 3. As these redshift ranges overlap nicely with those of the PFS, cross-correlating them can give additional cosmological information.

Combination of the lensing-galaxy cross-correlation and the RSD offers a powerful probe of modified gravity. This combination is called the "E_G estimator" (Zhang et al. 2007). It enables a gravity measure $\nabla^2(\psi - \phi)/f\delta_m$ free of uncertainties in the galaxy bias and matter fluctuations, by comparing the lensing-galaxy

cross-correlation and galaxy density-velocity correlation reconstructed from RSD. Existing E_G measurements (Reyes et al. 2010; Blake et al. 2016; Pullen et al. 2016; Alam et al. 2017; de la Torre et al. 2016) are limited to low redshifts, with large statistical uncertainties and potential systematics (Fig. 12). PFS in combination with HSC and ACT weak lensing will push the measurement to unprecedentedly high redshift ($0.6 < z < 2.4$), with unprecedentedly high accuracy ($\sim 5\%$ at 7 redshift bins). In the event that we find evidence for modified gravity such as "nDGP+DE" in the RSD data (Fig. 10), the measurement of E_G will be crucial in cross-checking such a ground-breaking discovery.

To be conservative we only used the large-scale information in Fig. 12: $\ell_{\rm max} = 350$ for $0.6 < z < 0.8$ and 780 for $2.0 < z < 2.4$. If smaller scale RSD and lensing measurements are included, the precision of E_G improves further.

Last but not least, cross-correlating PFS spectroscopic galaxies with photometric HSC galaxies allows us to calibrate photometric redshifts of the HSC galaxies, which in turn improves the cosmological analysis of HSC weak lensing measurements (Hikage et al. in preparation, also see Oguri & Takada 2011). Moreover, cross-correlation of the PFS galaxies with the lensing data of the HSC and the CMB lensing data allows us to calibrate various systematic effects inherent in each method and/or dataset (Schaan et al. 2017).

6. COMPETITION WITH DESI

PFS and DESI surveys are based on complementary philosophies: the former maps the large-scale structure with high fidelity (high number density) up to high redshifts over a smaller region in the sky, while the latter covers a much larger (10 times larger than PFS) region in the sky with limited redshift coverage (up to $z = 1.6$). This means that DESI's constraint on a constant equation of state of dark energy will be better than PFS: when both neutrino mass and w are varied, the expected 1-σ constraint on w is 0.037 for DESI and 0.051 for PFS. Nevertheless, PFS is still quite competitive because DESI needs 500 nights to achieve this, whereas PFS needs "only" 100 nights.

As for the neutrino mass constraint in ΛCDM, the expected 95% CL limits from PFS and DESI are comparable, i.e., 0.1 eV, because at this level of small neutrino mass they are both limited by the uncertainty in τ. Having two independent galaxy surveys covering different redshift ranges is powerful because we can cross-check the results that have profound implications for fundamental physics.

Still, it would be nice to get the results well before the first results of the DESI! This suggests that we "front-load" the PFS survey; namely, we complete our 100-night survey as soon as possible. In this way we can make a significant impact in the neutrino physics before DESI, and DESI would cross-check our results.

7. CONCLUSIONS

With 100 nights of the PFS cosmology survey program, we can make significant progress in our understanding of fundamental physics via constraints on the neutrino mass, time-evolving dark energy, and modification to GR on cosmological scales. This program is strengthened much further by exploiting the synergy with the HSC and CMB experiments in the overlapping regions.

We thank Chi-Ting Chiang and Donghui Jeong for the bispectrum calculations.

REFERENCES

Agrawal, A., Makiya, R., Chiang, C.-T., et al. 2017, JCAP, 10, 003

Alam, S., Miyatake, H., More, S., Ho, S., & Mandelbaum, R. 2017, MNRAS, 465, 4853

Allison, R., Caucal, P., Calabrese, E., Dunkley, J., & Louis, T. 2015, PhRvD, 92, 123535

Barreira, A., Sánchez, A. G., & Schmidt, F. 2016, PhRvD, 94, 084022

Bartolo, N., Komatsu, E., Matarrese, S., & Riotto, A. 2004, PhR, 402, 103

Blake, C., Joudaki, S., Heymans, C., et al. 2016, MNRAS, 456, 2806

Cai, Y.-C., Padilla, N., & Li, B. 2015, MNRAS, 451, 1036

Capak, P., Aussel, H., Ajiki, M., et al. 2007, ApJS, 172, 99

Cardamone, C., Schawinski, K., Sarzi, M., et al. 2009, MNRAS, 399, 1191

Chiang, C.-T., Wagner, C., Sánchez, A. G., Schmidt, F., & Komatsu, E. 2015, JCAP, 9, 028

Chiang, C.-T., Wagner, C., Schmidt, F., & Komatsu, E. 2014, JCAP, 5, 048

Chiang, C.-T., Wullstein, P., Jeong, D., et al. 2013, JCAP, 12, 030

Coil, A. L., Newman, J. A., Croton, D., et al. 2008, ApJ, 672, 153

Contreras, C., Blake, C., Poole, G. B., et al. 2013, MNRAS, 430, 924
Croft, R. A. C., Miralda-Escudé, J., Zheng, Z., et al. 2016, MNRAS, 457, 3541
Dalal, N., Doré, O., Huterer, D., & Shirokov, A. 2008, PhRvD, 77, 123514
D'Amico, G., Hamill, T., & Kaloper, N. 2016, PhRvD, 94, 103526
de la Torre, S., Jullo, E., Giocoli, C., et al. 2016, ArXiv e-prints, arXiv:1612.05647
Dodelson, S., Kaplinghat, M., & Stewart, E. 2000, Physical Review Letters, 85, 5276
Doran, M., & Robbers, G. 2006, JCAP, 6, 026
Dvali, G., Gabadadze, G., & Porrati, M. 2000, Physics Letters B, 485, 208
Frieman, J. A., Hill, C. T., Stebbins, A., & Waga, I. 1995, Physical Review Letters, 75, 2077
Hamaus, N., Cousinou, M.-C., Pisani, A., et al. 2017, JCAP, 7, 014
Hamaus, N., Pisani, A., Sutter, P. M., et al. 2016, Physical Review Letters, 117, 091302
Jouvel, S., Kneib, J.-P., Bernstein, G., et al. 2011, A&A, 532, A25
Komatsu, E., Afshordi, N., Bartolo, N., et al. 2009, astro2010: The Astronomy and Astrophysics Decadal Survey, arXiv:0902.4759
Laigle, C., McCracken, H. J., Ilbert, O., et al. 2016, ApJS, 224, 24
Lesgourgues, J., & Pastor, S. 2006, PhR, 429, 307
Matsuoka, Y., Onoue, M., Kashikawa, N., et al. 2016, ApJ, 828, 26
McAllister, L., Silverstein, E., & Westphal, A. 2010, PhRvD, 82, 046003
Mohapatra, R. N., Antusch, S., Babu, K. S., et al. 2007, Reports on Progress in Physics, 70, 1757
Morales, I., Montero-Dorta, A. D., Azzaro, M., et al. 2012, MNRAS, 419, 1187
Oguri, M., & Takada, M. 2011, PhRvD, 83, 023008
Pisani, A., Sutter, P. M., Hamaus, N., et al. 2015, PhRvD, 92, 083531
Planck Collaboration, Ade, P. A. R., Aghanim, N., et al. 2016, A&A, 594, A17
Pullen, A. R., Alam, S., He, S., & Ho, S. 2016, MNRAS, 460, 4098
Reyes, R., Mandelbaum, R., Seljak, U., et al. 2010, Nature, 464, 256
Sánchez, A. G., Scoccimarro, R., Crocce, M., et al. 2017, MNRAS, 464, 1640
Schaan, E., Krause, E., Eifler, T., et al. 2017, PhRvD, 95, 123512
Schmidt, F. 2009, PhRvD, 80, 123003
—. 2017, ArXiv e-prints, arXiv:1709.01544
Sefusatti, E., & Komatsu, E. 2007, PhRvD, 76, 083004
Silverstein, E., & Westphal, A. 2008, PhRvD, 78, 106003
Sunayama, T., Padmanabhan, N., Heitmann, K., Habib, S., & Rangel, E. 2016, JCAP, 5, 051
Sutter, P. M., Pisani, A., Wandelt, B. D., & Weinberg, D. H. 2014, MNRAS, 443, 2983
Takada, M., Ellis, R. S., Chiba, M., et al. 2014, PASJ, 66, R1
Xue, X.-X., Ma, Z., Rix, H.-W., et al. 2014, ApJ, 784, 170
Zehavi, I., Zheng, Z., Weinberg, D. H., et al. 2011, ApJ, 736, 59
Zhang, P., Liguori, M., Bean, R., & Dodelson, S. 2007, Physical Review Letters, 99, 141302
Zhao, G.-B., Crittenden, R. G., Pogosian, L., & Zhang, X. 2012, Physical Review Letters, 109, 171301
Zhao, G.-B., Raveri, M., Pogosian, L., et al. 2017, Nature Astronomy, 1, 627
Zhu, G., & Ménard, B. 2013, ApJ, 770, 130